Eur. Phys. J. C (2024) 84:245
https://doi.org/10.1140/epjc/s10052-024-12574-3

THE EUROPEAN PHYSICAL JOURNAL C

Regular Article - Theoretical Physics

A novel experimental search channel for very light higgs bosons in the 2HDM type I

S. Moretti[1,2], **S. Semlali**[1,3,a], **C. H. Shepherd-Themistocleous**[3]

[1] School of Physics and Astronomy, University of Southampton, Southampton SO17 1BJ, UK
[2] Department of Physics and Astronomy, Uppsala University, Box 516, 751 20 Uppsala, Sweden
[3] Particle Physics Department, Rutherford Appleton Laboratory, Chilton, Didcot, Oxon OX11 0QX, UK

Received: 13 October 2023 / Accepted: 18 February 2024 / Published online: 8 March 2024

Abstract We present a reinterpretation study of existing results from the CMS Collaboration, specifically, searches for light Beyond the Standard Model (BSM) Higgs pairs produced in the chain decay $pp \to H_{\rm SM} \to hh(aa)$ into a variety of final states, in the context of the CP-conserving 2-Higgs Doublet Model (2HDM) Type-I. Through this, we test the Large Hadron Collider (LHC) sensitivity to a possible new signature, $pp \to H_{\rm SM} \to ZA \to ZZh$, with $ZZ \to jj\mu^+\mu^-$ and $h \to b\bar{b}$. We perform a systematic scan over the 2HDM Type-I parameter space, by taking into account all available theoretical and experimental constraints, in order to find a region with a potentially visible signal. We investigate the significance of it through a full Monte Carlo simulation down to the parametrised detector level. We show that such a signal is an alternative promising channel to standard four-body searches for light BSM Higgs bosons at the LHC already with an integrated luminosity of $\mathcal{L} = 300$ fb^{-1}. For a tenfold increase of the latter, discovery should be possible over most of the allowed parameter space.

1 Introduction

One of the main goals of the LHC machine is to investigate the individual properties (mass, width, spin, CP quantum numbers) of the Higgs boson as well as its interactions (with both matter and forces) and to look into evidence for new physics. These features have been probed by the ATLAS and CMS collaborations in different production and decay channels, using proton-proton (pp) collision data collected at centre-of-mass energies of 7, 8 [1] and 13 TeV [2,3]. More recently, there have been observations involving the rare decay of the Higgs boson into a Z-boson and a photon ($H \to Z\gamma$) with a significance of 3.4σ [4], which could provide insights into the Higgs boson's coupling to both the electroweak gauge bosons and photons, contributing to our comprehension of the dynamics and interplays within the Higgs sector. Although the current measurements of the Higgs mass, spin, width and couplings to SM fermions and vector bosons [2,3] are all indeed in good agreement with the SM theoretical predictions, the small deviations in the SM-like Higgs couplings probed in various production modes for the five key decay channels $H \to \gamma\gamma$, ZZ^*, WW^*, $\tau\tau$ and $b\bar{b}$ [2,3] still provide signs of possible potential BSM contributions to the total Higgs width and hints of new physics through the invisible and/or undetected decays. The indirect constraints from the current fit of couplings measurements and direct searches for $H \to inv$ (i.e., to'invisible' final states) performed by ATLAS and CMS collaborations have placed upper limits on the Branching Ratio (BR) of Higgs boson to invisible particles and undetected BSM particles at 95% C.L. (Confidence Level) [5–8].

The quest to uncover the trilinear couplings also holds a prominent position on the LHC's research agenda. Such interactions can be probed with sufficient luminosity, although, at present (i.e., at the end of Run 2), they are not determined yet. A measurement of this interaction is one of the highest priority goals during, possibly, Run 3 and, certainly, at the High Luminosity LHC (HL-LHC), both of which would, therefore, start shedding light on the nature of the Higgs boson and the shape of the Higgs potential, which in turn has implications for the vacuum metastability, the hierarchy problem as well as the strength of the Electro-Weak (EW) phase transition. However, probing Higgs's self-interactions, both trilinear and quartic couplings, in multi-Higgs production is experimentally very challenging. From the theory side on the other hand, many models with an extended scalar sector, like the 2-Higgs Doublet model (2HDM) [9–13], the

[a] e-mail: souad.semlali@soton.ac.uk (corresponding author)

Next-to-2HDM
(N2HDM) [14–17] and a variety of both minimal and non-minimal Supersymmetric (SUSY) models [18–24] motivate additional features of new di-Higgs final states, as they all present with additional CP-even and/or -odd Higgs states, which can be accessible by the LHC experiments in a variety of signatures. Among the prominent processes are searches for exotic Higgs decays to a pair of light scalars or pseudo-scalars, e.g. $H \to aa, hh$, which then decay to SM particles.

This paper focuses on the popular 2HDM. After EW Symmetry Breaking (EWSB), the scalar sector of the 2HDM predicts five physical Higgs states, two CP-even Higgs bosons (h, H, with $m_h < m_H$), one CP-odd one (a) and a pair of charged ones ($H^\pm$). The rich (pseudo)scalar sector of the 2HDM and the different sets of Yukawa couplings that can be realised then offer a very interesting production and decay phenomenology of neutral and charged Higgs states at the LHC, even after scrutinising the 2HDM parameter space by considering different theoretical (vacuum stability, perturbativity, unitarity, etc.) and experimental (from SM-like Higgs data and null searches for companion states, flavour physics and low energy observables, etc.) constraints. Furthermore, the 2HDM is also attractive because one can impose a simple Z_2 discrete symmetry to the Yukawa sector in order to suppress Flavour Changing Neutral Currents (FCNCs) at tree level [25,26], which then forces one doublet to couple to a given type of fermions and leading as a result to four Yukawa interactions (termed, Type-I, Type-II, Type-X and Type-Y). In fact, in order to realise EWSB in such a way that the 2HDM is compliant with all experimental data, it is finally customary to allow for a soft breaking of this Z_2 symmetry. Herein, we will use the latter setup with a Type-I Yukawa structure. This particular scenario can accommodate both light neutral (10–100 GeV) and charged scalars (100–200 GeV), while one can not obtain such light Higgs states within the 2HDM Type-II or Type-Y configuration due ot the significant constraints arising from flavour physics, specifically from $B \to X_s\gamma$ which enforces a lower bound of 800 GeV on the charged Higgs mass [27].

In the present study, we plan to take advantage of the direct access to some trilinear Higgs couplings that the LHC can access, entering multi-Higgs processes such as $H \to hh(aa)$ and $H^\pm \to W^\pm a$, to test the sensitivity of the parameter space combination of 2HDM Type-I to light Higgs searches in cascade (or chain) decays. As the analysis progress, we aim to explore the scope of a new search for light Higgs bosons at the LHC Run 3 (with an integrated luminosity of 300 fb^{-1}) as well as the HL-LHC (with an integrated luminosity of 3000 fb^{-1}), on the basis of the knowledge acquired from the study of the aforementioned signatures. We focus mainly on the configuration of Type-I with inverted scenario, which in turn offers an alternative and new promising signal, in the form of the following cascade decays $H \to Z^*a \to Z^*Z^*h \to b\bar{b}\mu^-\mu^+jj$. The main Higgs production process is via gluon fusion $gg \to H$.

2 2HDM type-I

The 2HDM is one of the simplest well-motivated extensions of the SM. In this section, we briefly review the theoretical structure of this model. The scalar sector of the 2HDM consists of two complex $SU(2)_L$ doublets, Φ_1 and Φ_2, with hypercharge $Y = +1$. The most general $SU(2)_L \times U(1)_Y$ invariant scalar potential can be written as follows [11–13]:

$$\begin{aligned} V(\Phi_1,\Phi_2) = {} & m_{11}^2\Phi_1^\dagger\Phi_1 + m_{22}^2\Phi_2^\dagger\Phi_2 - [m_{12}^2\Phi_1^\dagger\Phi_2 + \text{h.c.}] \\ & + \frac{\lambda_1}{2}(\Phi_1^\dagger\Phi_1)^2 + \frac{\lambda_2}{2}(\Phi_2^\dagger\Phi_2)^2 \\ & + \lambda_3(\Phi_1^\dagger\Phi_1)(\Phi_2^\dagger\Phi_2) \\ & + \lambda_4(\Phi_1^\dagger\Phi_2)(\Phi_2^\dagger\Phi_1) + \left\{\frac{\lambda_5}{2}(\Phi_1^\dagger\Phi_2)^2 + \text{h.c.}\right\} \\ & + \left\{\left[\lambda_6(\Phi_1^\dagger\Phi_1) + \lambda_7(\Phi_2^\dagger\Phi_2)\right]\Phi_1^\dagger\Phi_2 + \text{h.c.}\right\}. \end{aligned} \tag{1}$$

Assuming CP-conservation in the 2HDM and following the hermiticity of the scalar potential, $m_{11}^2, m_{22}^2, m_{12}^2, \lambda_{1,2,3,4,5,6}$ are real parameters. Invoking the described Z_2 symmetry, to avoid tree-level Higgs-mediated FCNCs at tree level, implies that $\lambda_6 = \lambda_7 = 0$. Also notice that the bilinear term proportional to m_{12}^2 breaks the Z_2 symmetry softly. Using the two minimisation conditions of the scalar potential and the combination $v^2 = v_1^2 + v_2^2 = (2\sqrt{2}G_F)^{-1}$, one can then trade the Lagrangian parameters of the 2HDM for a more convenient set of variables,

$$\alpha,\ \tan\beta = \tfrac{v_2}{v_1},\ m_h,\ m_H\ ,\ m_a,\ m_{H^\pm}\ \text{ and }\ m_{12}^2,$$

where α is the CP-even mixing angle, v_1 and v_2 are the Vaccum Expectations Values (VEVs) of the two Higgs doublets Φ_1 and Φ_2, respectively.

2.1 Yukawa couplings

The general structure of the Yukawa Lagrangian when both Higgs fields couple to all fermions is given by [13]:

$$\begin{aligned} \mathcal{L}_Y = {} & \bar{Q'}_L(Y_1^u\tilde{\Phi}_1 + Y_2^u\tilde{\Phi}_2)u'_R + \bar{Q'}_L(Y_1^d\Phi_1 + Y_2^d\Phi_2)d'_R \\ & + \bar{L'_L}(Y_1^l\Phi_1 + Y_2^l\Phi_2)l'_R + \text{h.c.}, \end{aligned} \tag{2}$$

where Q'_L and L'_L are the weak isospin quark and lepton doublets, u'_R and d'_R denote the right-handed quark singlets while $Y_{1,2}^u$, $Y_{1,2}^d$ and $Y_{1,2}^l$ are couplings matrices in flavour space. This form of Yukawa interaction gives rise to large FCNCs at tree level, which is strongly constrained by B-physics observables. Implementing Z_2 symmetry [25,26] allows only one doublet to couple to a given right-handed fermion field.

Depending on the Z_2 assignment, one can have the four types of models previously refered to as Type-I, Type-II, Type-X and Type-Y. In the mass-eigenstate basis, they can be unified and expressed as follows:

$$\begin{aligned}-\mathcal{L}_Y = &+ \sum_{f=u,d,\ell} m_f \bar{f} f + \left(\frac{m_f}{v}\kappa_h^f \bar{f} f h + \frac{m_f}{v}\kappa_H^f \bar{f} f H\right) \\ &- i\frac{m_f}{v}\kappa_A^f \bar{f}\gamma_5 f A \\ &+ \frac{\sqrt{2}}{v}\bar{u}\left(m_u V \kappa_A^u P_L + V m_d \kappa_A^d P_R\right) d H^+ \\ &+ \frac{\sqrt{2} m_\ell \kappa_A^\ell}{v}\bar{\nu}_L \ell_R H^+ + \text{h.c.}, \end{aligned} \tag{3}$$

where $P_{L,R} = (1 \pm \gamma_5)/2$ are the projection operators and V denotes the Cabibbo–Kobayashi–Maskawa (CKM) matrix.

Here, we focus only on Type-I, where only one doublet Φ_2 couples to all fermions, and thus the Higgs-fermion couplings are flavour diagonal in the fermion mass basis and depend only on the mixing angles, α and β, as follows:

$$\begin{aligned}\kappa_h^{u,\,d,\,l} = c_\alpha/s_\beta,\ \kappa_H^{u,\,d,\,l} = s_\alpha/s_\beta, \\ \kappa_A^u = \cot\beta,\ \kappa_A^{d,\,l} = -\cot\beta,\end{aligned}$$

where we have used the short-hand notation c and s for cos and sin, respectively.

2.2 Theoretical and experimental constraints

We now describe briefly a set of, in turn, theoretical and experimental constraints that must be satisfied by the parameter space of the 2HDM.

- Perturbative unitarity constraints require a variety of tree-level 2-to-2 body scatterings processes (e.g. scalar-scalar, gauge boson-gauge boson and scalar-gauge boson) to remain unitary at high energy [28–30].
- Vacuum stability [31] requires the scalar potential to be finite at large field values, leading to the following bounds:

$$\lambda_{1,2} > 0,\ \lambda_3 > -\sqrt{\lambda_1\lambda_2},\ \lambda_3 + \lambda_4 - |\lambda_5| > -\sqrt{\lambda_1\lambda_2}.$$

- Perturbativity requires the quartic couplings to obey $|\lambda_i| < 4\pi$ $(i = 1, \ldots, 5)$.

The above constraints have been implemented in `2HDMC-1.8.0` [32]. This public code is then used to explore the 2HDM parameter space and to compute the different Higgs BRs in each point of it. (`2HDMC` also provides an interface to `HiggsBounds` and `HiggsSignals`, see below.)

Experimental observations impose the following constraints:

- EW precision observables, i.e., the oblique parameters, S, T and U [33,34] are required to be within 95% C.L. of their experimental measurements, the current fit values (with the correlation parameters) are given by [35]:

$$\begin{aligned}S = -0.02 \pm 0.10,\ \ T = 0.03 \pm 0.12, \\ U = 0.01 \pm 0.11,\ \ \rho_{ST} = 0.92,\ \ \rho_{SU} = -0.80, \\ \rho_{TU} = -0.93,\ \ \chi_{ST,\,SU,\,TU} < 5.99.\end{aligned}$$

- Consistency with the Z width measurement $\Gamma_Z = 2.4952 \pm 0.0023$ GeV from LEP [36,37] is required.
- Constraints from LHC, Tevatron and LEP searches which failed to find companion Higgs states are taken into account via `HiggsBounds-5.10.0` [38], which allows to test the exclusion limits at 95% C.L.
- The code `HiggsSignals-2.6.2` [39] is used to check the signal strength measurements of the SM-like Higgs boson discovered at the LHC in 2012.
- Constraints from B meson decays are enforced by Superiso-v1.4 [40], using the current measurements:
  - $\text{BR}(\overline{B} \to X_s\gamma)|_{E_\gamma < 1.6\text{ GeV}} = (3.32 \pm 0.15) \times 10^{-4}$ [41],
  - $\text{BR}(B_s \to \mu^+\mu^-)_{(\text{LHCb})} = \left(3.09^{+0.46}_{-0.43}\right) \times 10^{-9}$ [42,43],
  - $\text{BR}(B_s \to \mu^+\mu^-)_{(\text{CMS})} = \left(3.83^{+0.38}_{-0.36}\right) \times 10^{-9}$ [44],
  - $\text{BR}(B^0 \to \mu^+\mu^-)_{(\text{LHCb})} = \left(1.2^{+0.8}_{-0.7}\right) \times 10^{-10}$ [42,43],
  - $\text{BR}(B^0 \to \mu^+\mu^-)_{(\text{CMS})} = \left(0.37^{+0.75}_{-0.67}\right) \times 10^{-10}$ [44].
- Constraints from recent searches for light pseudoscalar states in the mass range [15, 62.5] GeV, in proton-proton collision at $\sqrt{s} = 13$ TeV, in $\mu^+\mu^- b\bar{b}$ [45,46], $\mu^+\mu^-\tau^+\tau^-$ [47] and $\tau^+\tau^- b\bar{b}$ [48] final states, are included in `HiggsBounds`. Since no significant excess is observed, upper limits are set on $\text{BR}(H \to aa \to \mu^+\mu^- b\bar{b},\ \mu^+\mu^-\tau^+\tau^-,\ \tau^+\tau^- b\bar{b})$ [45–48]. However, lately, additional constraints from such Higgs cascade decays have emerged, not included in the numerical tool, so we had to deal with these separately. For example, the CMS group has reported a search for $H \to aa \to 4\gamma$ [49], using the data collected at $\sqrt{s} = 13$ TeV, with an integrated luminosity of 132 fb^{-1}. Upper limits can then be set on $\text{BR}(H \to aa \to 4\gamma)$ at 95% C.L, since no significant deviation is observed.[1] The ATLAS

[1] EasyNData [50] was used to digitise the exclusion limits from the published papers in order to test each point in the parameter space against the upper limit on $\text{BR}(H \to hh(aa) \to 4\gamma)$ [49], a

Table 1 (×)/(✓) indicate searches (not yet)/(already) implemented in `HiggsBounds-5.10.0`

Limit	Collaboration	Range	HiggsBounds
$H \to aa \to \mu^+\mu^- b\bar{b}$ [45]	CMS	15 GeV $< m_a <$ 60 GeV	✓
$H \to aa \to \mu^+\mu^- b\bar{b}$ [46]	ATLAS	15 GeV $< m_a <$ 60 GeV	✓
$H \to aa \to \mu^+\mu^-\tau^+\tau^-$ [47]	CMS	15 GeV $< m_a <$ 61.5 GeV	✓
$H \to aa \to \tau^+\tau^- b\bar{b}$ [48]	CMS	15 GeV $< m_a <$ 60 GeV	✓
$H \to aa \to 4\gamma$ [49]	CMS	15 GeV $< m_a <$ 60 GeV	×
$H \to aa \to \mu^+\mu^- b\bar{b}$ [51]	CMS	15 GeV $< m_a <$ 60 GeV	×
$H \to aa \to \tau^+\tau^- b\bar{b}$ [51]	CMS	15 GeV $< m_a <$ 60 GeV	×
$H \to aa \to \mu^+\mu^-\tau^+\tau^-$ [52]	CMS	3.6 GeV $< m_a <$ 21GeV	×
$H \to aa \to \mu^+\mu^- b\bar{b}$ [53]	ATLAS	15 GeV $< m_a <$ 60 GeV	×

group [53] has also recently searched for the exotic decay of the Higgs boson into two light pseudoscalars in $\mu^+\mu^- b\bar{b}$ final state at $\sqrt{s} = 13$ TeV with an integrated luminosity of 137 fb^{-1}, in the range of masses varying from 15 to 60 GeV. An upper limit is placed on BR($H \to aa \to \mu^+\mu^- b\bar{b}$)[2] at 95%C.L. Table 1 summarises several searches for exotic decays of the Higgs bosons in various final states, performed by the two collaborations ATLAS and CMS at Run 2, targeting a different ranges of masses.

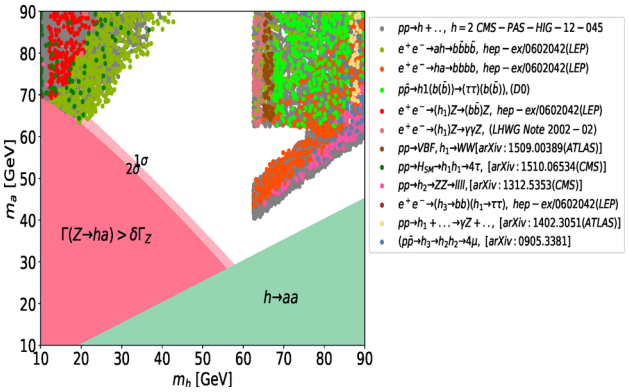

Fig. 1 Allowed parameter space in the 2HDM Type-I at 95% C.L. The solid red and green regions are excluded by the Z width constraint and the LEP search for $h \to aa$ [54], respectively. The most sensitive searches for the relevant (m_h, m_a) regions are shown by coloured dots. Each coloured point in the (m_h, m_a) plane satisfies all theoretical requirements and up-to-date experimental constraints. In the white space, any combination of masses is ruled out by current experimental searches

3 Numerical analyses

The (pseudo)scalar sector of the 2HDM involves two CP-even Higgs bosons, h and H. One of these scalars can be identified as the 125 GeV state observed at the LHC. As mentioned, in this analysis, we will assume that the heaviest Higgs state H is the SM-like one with a mass of 125 GeV and that h and a are lighter than H. We the perform a scan over the following ranges,

$$\begin{aligned} &m_h \in [10\text{ GeV},\ 90\text{ GeV}],\ m_H = 125\text{ GeV},\\ &m_a \in [10\text{ GeV},\ 90\text{ GeV}],\ m_{H^\pm} \in [100\text{ GeV},\ 160\text{ GeV}],\\ &\tan\beta \in [2.5,\ 25],\ \ \sin(\beta-\alpha) \in [-0.7,\ 0.0], \end{aligned} \tag{4}$$

with $m_{12}^2 = m_a^2 \tan\beta/(1+\tan^2\beta)$. Assuming $m_H = 125$ GeV and $m_{h,a} < 90$ GeV, the decay channels $H \to hh, aa, aZ^*$ could be open, leading to invisible or undetected SM-like Higgs decays that are restricted by the current precision measurements of Higgs couplings. CMS performed a combination of searches, using data collected at $\sqrt{s} = 7,\ 8,\ 13$ TeV [7], for Higgs bosons decaying into invisible particles, which targets the following production channels: Vector Boson Fusion (VBF), Higgs-Strahlung (HS) and gluon-gluon Fusion (ggF) (allowing for initial state radiation). The combination of all the searches, assuming these SM-like production modes, yields an observed (expected) upper limit on BR($H \to inv$) of 0.19 (0.15) at 95% C.L. The ATLAS group reported a direct search for Higgs bosons produced via VBF with subsequent invisible decays, for 139 fb^{-1} of pp collision data at $\sqrt{s} = 13$ TeV [8]. An observed (expected) upper limit of 0.145 (0.103) is placed on BR($H \to inv$) at 95% C.L., as a function of the assumed production cross sections. As for now, both ATLAS and CMS have placed, respectively, an upper bound of 0.10 [6] and 0.15 [5] on BR($H \to$ invisible) at 95% CL. In our analysis, we will assume that BR($H \to inv$) designates the sum of the following decay rates, BR($H \to hh$), BR($H \to aa$) and BR($H \to aZ^*$).

After performing a random scan over 2HDM Type-I parameters, we show in Fig. 1 the allowed regions by the-

Footnote 1 continued
procedure which was validated against the case of BR($H \to hh(aa) \to \mu^+\mu^- b\bar{b}$[51], $\tau^+\tau^- b\bar{b}$ [51], $\mu^+\mu^-\tau^+\tau^-$ [52], $\mu^+\mu^- b\bar{b}$ [53].

[2] Corresponding search data and exclusion limits are available at the HEPData database.

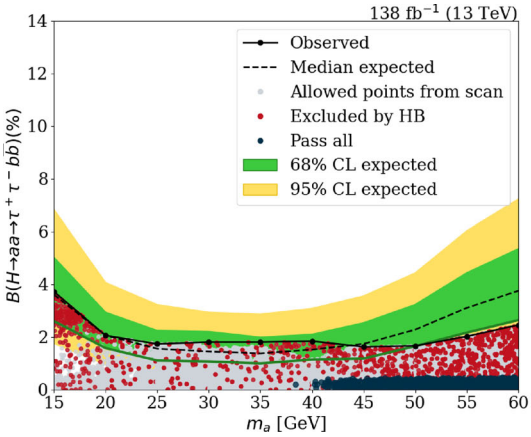

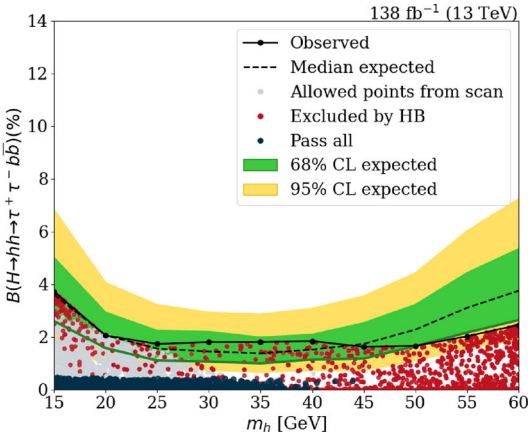

Fig. 2 Observed and expected upper limits on $B(H \to aa(hh) \to \tau^+\tau^-b\bar{b})$ [51] at 95% C.L. in the 2HDM Type-I. Grey points are allowed by theoretical constraints. As stated above, red colour indicates the combination of the scanned model parameters, which is excluded by existing experimental searches checked by HiggsBounds [38], whereas blue points satisfy both theoretical and experimental constraints

oretical and experimental constraints. The figure also captures the constraint from the Z width (bottom-left red region), which forbids possible mass combinations $(m_h,\ m_a)$ when $\cos(\beta-\alpha) \to 1$. Additionally, the constraint from the LEP search for the $e^+e^- \to (h \to aa)a \to (b\bar{b}b\bar{b})b\bar{b}$ process [54] excludes the bottom-right region corresponding to $m_h > 2m_a$, where the decay channel $h \to aa$ is kinematically open (bottom-right green region).

Each (coloured) point in the (m_h, m_a) plane implies that there is a combination of the scanned model parameters, which obeys the aforementioned theoretical constraints and evades the current experimental limits in all searched modes, whereas the white space corresponds to the case where any possible mass combination is forbidden by an observed signature(s) in one or more existing experimental searches.

Within this region, the most sensitive channels for the model parameter points, as determined by `HiggsBounds`, are shown by coloured dots. Note that each coloured point in the parameter space of the 2HDM is allowed by current experimental searches. Obviously, there are two distinct regions in the figure. The one in the top left corner corresponds to low masses of h ($m_h < m_H/2$), and high masses of a ($m_a > m_H/2$), while the second one corresponds to the $m_{a,\,h} > m_H/2$ scenario. It is interesting to note that there are no acceptable points when 40 GeV $< m_h < m_H/2$ and $m_a > m_H/2$. This is due to the fact that this parameter combination is excluded by LEP searches for $e^+e^- \to ah \to b\bar{b}b\bar{b}$ [54] and an ATLAS search for events with at least 3γ in $pp \to H_{\rm SM} \to hh \to 4\gamma$ [55].

Finally, it is noteworthy that the most sensitives searches for the region with low m_h and high m_a are the LEP searches for processes such as $e^+e^- \to ah \to b\bar{b}b\bar{b}$ and $e^+e^- \to (h)Z \to (b\bar{b})Z$ [54]. Therefore, an update from the LHC during Run 3 is unlikely to rule out this mass combination over the plane $(m_h,\ m_a)$ of the 2HDM Type-I. We will be focusing on this region in the second part of our study.

We now turn to the reinterpretation of exotic Higgs decay searches, i.e., $H \to aa$ in $\tau^+\tau^-b\bar{b}$, $\mu^+\mu^-b\bar{b}$ and $\mu^+\mu^-\tau^+\tau^-$ final states in the framework of the 2HDM Type-I, while taking advantage of the parameter space discussed above. The recasting of $\tau^+\tau^-b\bar{b}$, $\mu^+\mu^-b\bar{b}$ and $\mu^+\mu^-\tau^+\tau^-$ searches for $H \to hh$ is also possible since these processes share similar kinematics (in the same spirit as in Ref. [56]). It is relevant to note that the constraints from the search for light pseudoscalars in the $\tau^+\tau^-b\bar{b}$ final state are much stronger than the ones from $\mu^+\mu^-b\bar{b}$ and $\mu^+\mu^-\tau^+\tau^-$ searches. CMS has set an upper limit, between 1.7% and 7.6%, on BR$(H \to aa \to \tau^+\tau^-b\bar{b})$ at 95% C.L. [51], assuming the SM production of primary Higgs boson. We show in Fig. 2 the outcome from reinterpreting the $H \to aa(hh) \to \tau^+\tau^-b\bar{b}$ search [51] in the 2HDM Type-I. The yellow and green bands represent the uncertainties at $\pm1\sigma$ and $\pm2\sigma$ associated with the expected exclusion limits. Grey points satisfy theoretical constraints described in Sect. 2.2, whereas red points are excluded by null searches (i.e., by `HiggsBounds` [38]). The blue points satisfy both theoretical and experimental constraints. The area of sensitivity to $H \to aa(hh) \to \tau^+\tau^-b\bar{b}$ is already excluded by existing experimental searches (red points). In this connection, the BR of Higgs SM-like Higgs state decaying into hh and/or aa is very restricted and cannot exceed 9% at 95% C.L., again, in the 2HDM Type-I.

One can draw a similar conclusion form reinterpreting $H \to hh(aa) \to \mu^+\mu^-b\bar{b}$ [51] in our reference framework. Figure 3 shows that the parameter space with sensitivity to this search is excluded. One should keep in mind that the $\mu^+\mu^-b\bar{b}$ final state is well-balanced between large BR$(h/a \to b\bar{b})$ and a clean di-muon resonance that is easy

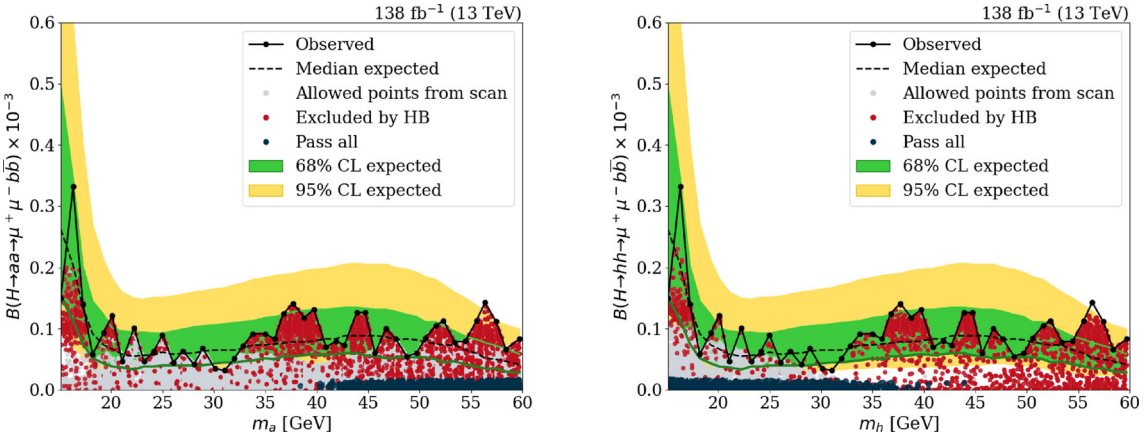

Fig. 3 Observed and expected upper limits on $B(H \to aa(hh) \to \mu^+\mu^- b\bar{b})$ [51] at 95% C.L. in the 2HDM Type-I

to trigger on. This exercise emphasises that the 2HDM Type-I may not be a good framework for reinterpreting searches for exotic Higgs decays into light pseudoscalar in "traditional" final states such as $\mu^+\mu^- b\bar{b}$, $\tau^+\tau^- b\bar{b}$ and $\mu^+\mu^-\tau^+\tau^-$.

We also address here light charged Higgs decay in the mass ranges where $m_{H^\pm} < m_t - m_b$ and $m_{h,a} < 90$ GeV. In this configuration, the charged Higgs state can be be produced from top quark decays, i.e., $t \to bH^+$, followed by its bosonic decays to $H^\pm \to W^\pm h(a)$, instead of the standard fermionic decay modes like $\tau\nu$ and cs. Many studies motivated these channels as alternative modes to search for light charged Higgs bosons that could dominate over the conventional fermionic channels, because of large BRs when they are kinematically allowed, in models such as our 2HDM Type-I [57–60]. ATLAS [61] and CMS [62] have considered the ranges $m_a \in [15, 75]$ GeV and $m_{H^\pm} < m_t - m_b$ to search for light charged Higgs bosons in $pp \to t\bar{t} \to b\bar{b}H^+W^-$ with $H^+ \to W^+a$ and $a \to \mu^+\mu^-$ at $\sqrt{s} = 13$ TeV, since the $\mu^+\mu^-$ finale state provides the aforementioned experimental advantages, which offset the suppressed rate of BR$(a \to \mu^+\mu^-)$. Previously, both CDF and the LEP collaborations have searched for $H^\pm \to W^\pm a$ with $a \to b\bar{b}$ [63], $a \to \tau^+\tau^-$ [64] and $a \to b\bar{b}$ [65]. In addition, LEP experiments [66] have set a lower bound on the charged Higgs boson mass of $m_{H^\pm} > 72.5$ GeV in the 2HDM Type-I for $m_a > 12$ GeV at 95% C.L.

Figure 4 shows the CMS observed and expected exclusion limits on the product of the BRs of $t \to bH^\pm$, $H^\pm \to W^\pm a$ and $a \to \mu^+\mu^-$ [62] as a function of m_a predicted by the 2HDM Type-I, with respect to several theoretical and experimental constraints. We adopt here $m_{H^\pm} = m_a + 85$ GeV [62], which enables us to consider $H^\pm \to W^{\pm(*)}a$, with $W^{\pm(*)}$ being on/off shell, by randomly sampling values of the charged Higgs mass between 100 GeV and 160 GeV (see Eq. (4)). A noteworthy observation is that the 2HDM Type-I offers sufficient sensitivity, when the prediction of

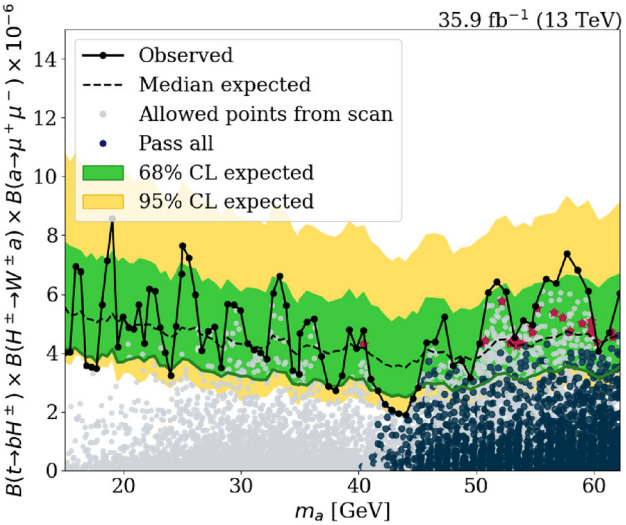

Fig. 4 Observed and expected upper limits on BR$(t \to H^+b) \times$ BR$(H^+ \to W^+a) \times$ BR$(a \to \mu^+\mu^-)$ [62] at 95% C.L. in the 2HDM Type-I

the model exceeds the expected limit produced at $\sqrt{s} = 13$ with an integrated luminosity of 35.9 fb^{-1} (purple stars). Such a signature could be exploited to search for a light $H^\pm$ at future experiments, Run 3 and/or the HL-LHC, given the available energies and luminosities by then. Therefore, we present in Table 2 some Benchmark Points (BPs) to test the actual sensitivity of these experiments to the 2HDM Type-I parameter space.

We move now to discuss a new analysis, where we deploy the parameter space of the 2HDM Type-I following the outcomes of reinterpreting previous searches for light Higgs bosons, $pp \to H_{\rm SM} \to hh(aa)$, in different final states, in order to search for a new signature.

Figure 5 shows the result of performing a scan over the parameter space of 2HDM Type I, wherein (recall) the heav-

Table 2 BPs in the 2HDM Type-I

Parameters	BP1	BP2	BP3	BP4
(Masses are in GeV)				
m_h	62.86	75.69	75.58	77.18
m_H	125	125	125	125
m_a	40.37	50.73	52.90	53.44
$m_{H^\pm}$	105.19	108.15	110.83	111.95
$\tan\beta$	4.82	4.73	4.58	4.57
$\sin(\beta-\alpha)$	−0.203	−0.209	−0.220	−0.0.215
Total decay width in GeV				
$\Gamma(h)$	1.9×10^{-6}	3.00×10^{-6}	1.9×10^{-6}	3.00×10^{-6}
$\Gamma(H)$	4.54×10^{-3}	4.53×10^{-3}	4.47×10^{-3}	4.48×10^{-3}
$\Gamma(A)$	5.39×10^{-5}	6.79×10^{-5}	7.6×10^{-5}	7.7×10^{-5}
$\Gamma(H^\pm)$	3.31×10^{-4}	3.330×10^{-4}	3.339×10^{-4}	3.339×10^{-4}
$\mathrm{BR}(A\to XY)$				
$\mathrm{BR}(A\to\mu\mu)$	2.36×10^{-4}	2.42×10^{-4}	2.43×10^{-4}	2.43×10^{-4}
$\mathrm{BR}(H^\pm\to XY)$ in %				
$\mathrm{BR}(H^\pm\to W^+A)$	86.65	90.64	88.47	89.39

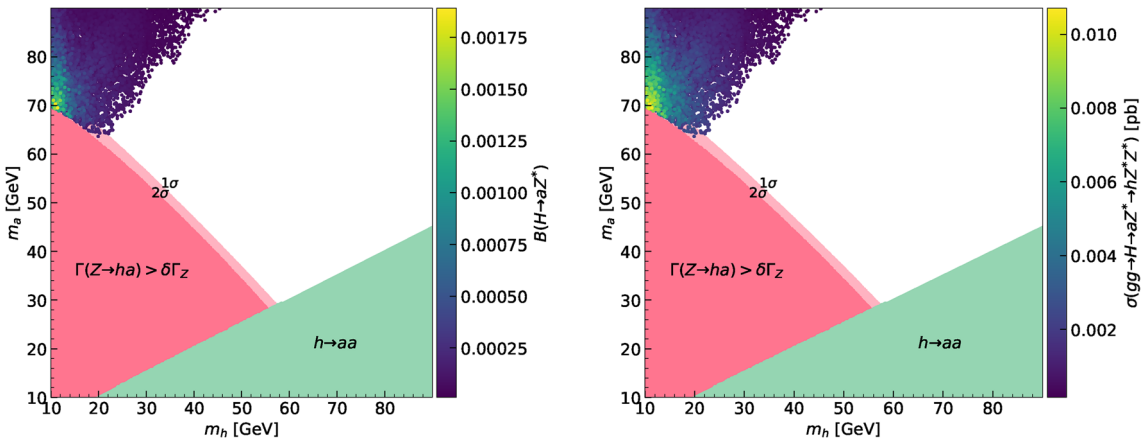

Fig. 5 m_h and m_a vs. $\mathrm{BR}(H\to Z^*a)$ (left) and $\sigma(gg\to H\to Z^*a\to Z^*Z^*h)$ (right) at 95% C.L. in the 2HDM Type-I

iest Higgs state is identified as the discovered SM-like one. Each sampled point is required to satisfy the theoretical and experimental constraints described in Sect. 2.2. In the left panel, we illustrate m_a vs. m_h with the BR of $H\to aZ^{(*)}$ on the colour gauge. Since $m_H/2 < m_a < 125$ GeV, $H\to aZ^{(*)}$ will proceed with Z being off-shell, which explains the suppressed BR ($< 0.2\%$). In this configuration, $H\to aa$ will not be open, thus, $H\to hh$ would only contribute significantly to the undetected decays of H. It should be pointed out that the total amount of $\mathrm{BR}(H\to aa^*+aZ^*+hh)$ should not exceed 12% as required by $\mathrm{BR}(H\to inv)$ [2]. In the right panel, we show m_a as a function of m_h with $\sigma(H\to aZ^*\to hZ^*Z^*\to Z^*Z^*)$ on the colour gauge. Once the decay chain $H\to aZ^*$ is open, the subsequent decay of a could lead to $a\to Z^*h$ with Z being off-shell and h decaying to fermions and/or $\gamma\gamma$. We use `Sushi` [67–69] to compute the cross section of Higgs production at LO.[3] It is worth highlighting that Figs. 5, 6 and 14 focus particularly on the region characterized by small m_h and large m_a in contrast to Fig. 1, which displays both regions. The cross-section of our signature, i.e., $gg\to H\to aZ^*\to h(\to b\bar{b})Z^*Z^*$, is remarkably negligible in the region with large m_h and m_a ($m_h > 60$ GeV and $m_a > 40$ GeV), primarily due to the fact that the pseudoscalar decay width (Γ_a) is dominated by $a\to b\bar{b}$ with a branching ratio of 85%, rather than $a\to Z^*h$. Note that the contribution of $a\to b\bar{b}$ is negligible in the region with low m_h and high m_a. Instead, the predominant channel in this region is $a\to Z^*h$ with Z being off-shell, boasting a branching ratio that can reach 90%. Furthermore,

[3] The signal cross sections is computed at LO (i.e, tree level) here, however, we will consider QCD corrections through K-factors later on in our study.

the decay of $H_{SM} \to aZ^*$ is suppressed in the region with large m_h and m_a. In fact, H_{SM} tends to decay to aZ^* in the specific part of the region where the observation of $a \to Z^*h$ is not possible.

We show in Fig. 6 the $gg \to H \to aZ^* \to hZ^*Z^*$ cross section, where $h \to b\bar{b}$. The process could yield a cross section of 0.006 pb. In the right panel of Fig. 6 we show the BR of $h \to b\bar{b}$ in this region of the 2HDM Type-I parameter space. Obviously, the decay width of h is dominated by the decay mode $h \to b\bar{b}$. Thus, in what follows, we focus on the case where h decays to $b\bar{b}$ and $Z^{(*)}Z^{(*)} \to \mu^+\mu^- jj$. Such a scenario could be an alternative channel to search for light Higgs bosons at Run 3 and the HL-LHC.

4 Signal vs. background analysis

We describe here the toolbox used to generate and analyse MC events. `MadGraph-v.9.2.5` [70] is used to generate parton level configurations of both signal and background processes.[4] The events are passed then to `PYTHIA8` [72] to simulate parton showering, hadronisation and decays. Finally, we use `Delphes-3.5.0` [73] with the standard CMS card[5] to perform detector simulation. We resort to `MadAnalysis` [74] to apply cuts and to conduct the analysis.

The major background processes are top pair production in association with 2 Initial State Radiation (ISR) jets,[6] ZZ production with additional $b\bar{b}$ quarks, $ZW + b\bar{b} \to \mu^+\mu^- jjb\bar{b}$ and Drell-Yan plus jets (DY+jets). We show in Table 3 the corresponding cross sections at $\sqrt{s} = 13$ TeV for the LHC energy. We have generated MC samples of (10^6) events. Unsurprisingly, the irreducible backgrounds $pp \to Z^{(*)}Z^{(*)}b\bar{b} \to b\bar{b}jj\mu^+\mu^-$ (from both QCD and EW interactions) and $pp \to ZWb\bar{b} \to b\bar{b}jj\mu^+\mu^-$ are negligible whereas $pp \to gg t\bar{t} \to gg\mu^+\mu^- jjb\bar{b}\nu_\mu\bar{\nu}_\mu$ and DY+jets are large.

We considered a few BPs for the signal given by $gg \to H \to aZ^* \to hZ^*Z^* \to \mu^+\mu^-\ jj\ b\bar{b}$ to perform the MC simulation. The input parameters of each BP are given in Table 4. Note that the light Higgs width, $\Gamma(h)$, is not small enough to lead to a large lifetime and hence, long-lived particles producing displaced vertices inside the detector. The proper decay length $c\tau_0$ is in fact only a tiny fraction of micrometers.[7] The different kinematic distributions at parton level in Fig. 7 show that the requirement of central pseudo-rapidity of the muons is generally satisfied however the p_T of these can be rather small. To address this, one can invoke the di-muon scouting trigger,[8] which involves lowering the transverse momentum (p_T^μ) of muons to 4.5 GeV [77,78]. Note that the p_T threshold of such trigger is reduced to 3 GeV [79] in Run 3. Figure 8 shows the invariant mass distributions of the two b-jets, $m_{b\bar{b}}$, and that of the full final state, $m_{jj\mu^+\mu^-b\bar{b}}$, for the signal and the irreducible background processes at parton level, noting that $m_{b\bar{b}}$ is close to light Higgs mass m_h and $m_{jj\mu^+\mu^-b\bar{b}}$ is close to SM-like Higgs mass m_H (for the signal, unlike the irreducible backgrounds). We will clearly leverage these underlying partonic shapes in our detector level[9] analysis, to which we proceed next, in the presence of the following sequence of acceptance cuts:

$$p_T^b > 20\ \text{GeV},\ p_T(j) > 20\ \text{GeV},\ p_T^{\mu_1} > 10\ \text{GeV},$$
$$p_T^{\mu_2} > 5\ \text{GeV},\ |\eta(l,b)| < 2.5,\ |\eta(j)| < 5.0,\ \Delta R > 0.4.$$

Additionally, we only consider events with two oppositely charged muons, two b-jets and two light jets in the final state. Events are further preselected after requiring the invariant mass of the two b-jets ($m_{b\bar{b}}$), the two light jets (m_{jj}) and the di-muon system[10] ($m_{\mu\mu}$) to lie within the following mass ranges, as shown in Fig. 9,

$$5\ \text{GeV} < m_{b\bar{b}} < 40\ \text{GeV},\ 10\ \text{GeV} < m_{\mu\mu} < 50\ \text{GeV},$$
$$10\ \text{GeV} < m_{jj} < 50\ \text{GeV}.$$

Figure 10 displays the distributions of the missing transverse energy ($\not{E}_T$) and the highest p_T's of b-jets, light-jets and muons for signal and background processes at detector level. (As mentioned previously, the irreducible backgrounds stemming from $ZZb\bar{b}$ and $ZWb\bar{b}$ processes are negligible, so we have not emulated these at detector level.)

[4] Background and signal events are generated at LO. Higher order corrections are quantified through K-factors. The NLO QCD correction to top pair production in association with 2 jets computed at the LHC is about -27% [71], which we adopt here. The NLO corrections to $gg \to H$ are very large , about a facor of 2, due to the contributions from gg pairs to QCD radiation, whereas $K_{\text{NNLO/NLO}} \approx$ is much smaller than $K_{\text{NLO/LO}}$, signifying a convergence of the QCD expansion, so we renormalise the signal to the NNLO rates through the K-factor $K_{\text{NNLO/LO}} = \sigma^{\text{NNLO}}/\sigma^{\text{LO}} \sim 2.6 - 2.7$.

[5] It adopts the anti-k_T algorithm to cluster final particles into jets, with jet parameter $\Delta R = 0.5$ and $p_{T,j}^{\min} = 20$ GeV (for both light and b jets)

[6] In our study, we focus mainly on $gg t\bar{t}$ which is vastly dominant over $gq\bar{q}t\bar{t}$ and $q\bar{q}t\bar{t}$.

[7] The proper decay length $c\tau_0$ falls within the range from $0.06\mu m$ to $0.19\mu m$, where τ_0 is the light Higgs lifetime at rest [75].

[8] The CMS standard dimuon triggers require the highest p_T muon to possess a transverse momentum within the range of 12-17 GeV, while the second-highest p_T muon reconstructed should exhibit a p_T between 5-8 GeV [76]. This consequently leads to a significant loss of signal acceptance in searches for dimuon masses below 40 GeV [77,78].

[9] The minimum p_T requirements for muons has been lowered to 5 GeV to cover the entire signal region effectively. This modification is implemented in the Delphes card to simulate the CMS detector.

[10] Both $\mu\mu$ and jj originate from the decays of off-shell Z bosons ($Z^*Z^* \to \mu^+\mu^- jj$).

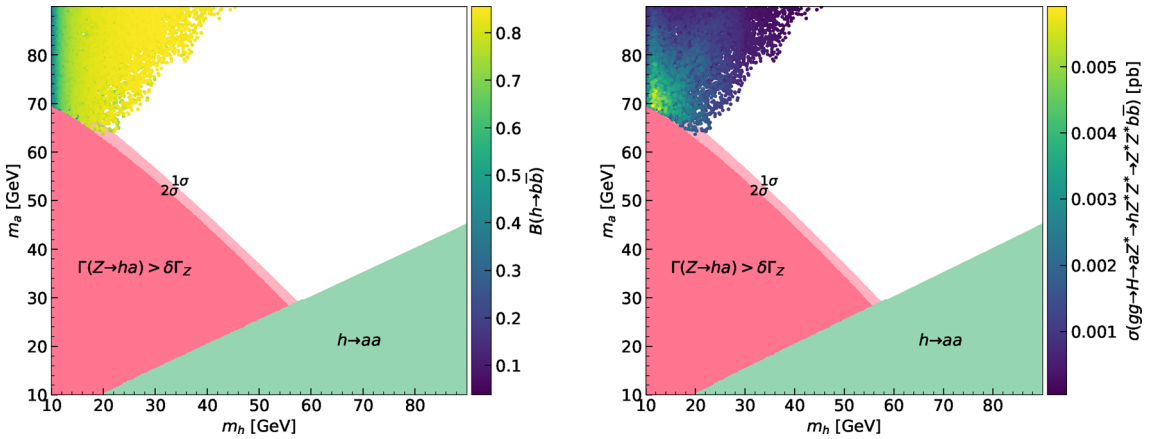

Fig. 6 m_h and m_a vs. BR($h \to b\bar{b}$) (left) and $\sigma(gg \to H \to aZ^* \to hZ^*Z^* \to Z^*Z^*b\bar{b})$ (right) at 95% C.L. in the 2HDM Type-I

Table 3 The parton level cross sections of the background processes at LO

Background	Cross section (pb)
$pp \to ZZb\bar{b}_{\text{QCD}} \to \mu^+\mu^- jjb\bar{b}$	$7.29 \times 10^{-4} \pm 1.9 \times 10^{-6}$
$pp \to ZZb\bar{b}_{\text{QED}} \to \mu^+\mu^- jjb\bar{b}$	$8.39 \times 10^{-5} \pm 2 \times 10^{-7}$
$pp \to ggt\bar{t} \to gg\mu^+\mu^- jjb\bar{b}\nu_\mu\bar{\nu}_\mu$	1.7 ± 0.008
DY + jets ($\mu^+\mu^- jjb\bar{b}$)	3.2 ± 0.0039
$pp \to ZW^+b\bar{b}, W^+ \to jj$	$3.13 \times 10^{-4} \pm 7.9 \times 10^{-7}$
$pp \to ZW^-b\bar{b}, W^- \to jj$	$2.84 \times 10^{-4} \pm 6.3 \times 10^{-7}$

Table 4 Selected BPs with parton level cross section and other observables at LO. (All masses and widths are in GeV, with $m_H = 125$ GeV.)

BPs	m_h	m_a	$m_{H^\pm}$	$\sin(\beta-\alpha)$	$\tan\beta$	$\Gamma(h)$	$\Gamma(H)$	$\Gamma(A)$	$\Gamma(H^\pm)$	$\Gamma(Z\to ha)$	σ (pb)
BP1	15.37	72.21	120.99	−0.19	8.55	3.11×10^{-9}	4.4×10^{-3}	1.028×10^{-4}	7.88×10^{-2}	0.00083	3.28×10^{-4}
BP2	12.56	74.12	113.93	−0.16	5.97	1.01×10^{-9}	4.4×10^{-3}	1.60×10^{-4}	4.752×10^{-2}	0.000968	4.11×10^{-4}
BP3	11.64	73.03	104.56	−0.19	5.09	3.13×10^{-9}	4.49×10^{-3}	1.644×10^{-4}	3.96×10^{-2}	0.00164	4.73×10^{-4}

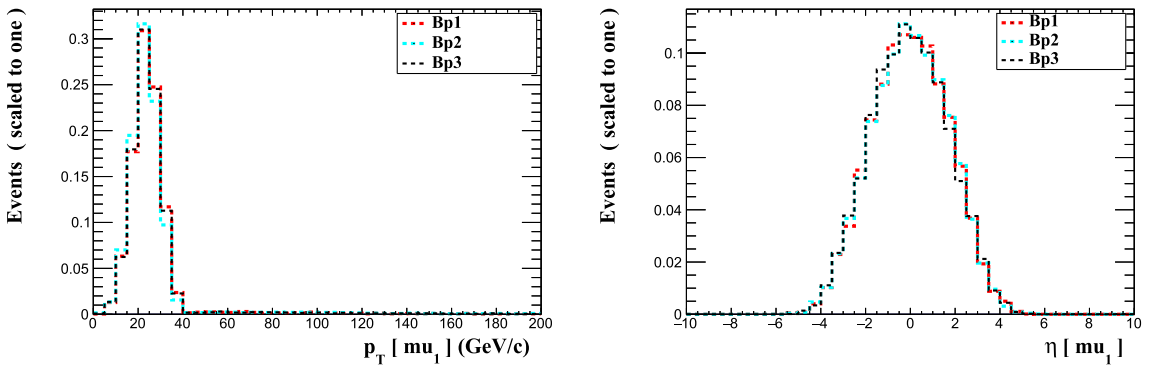

Fig. 7 The transverse momentum (left) and pseudorapidity (right) of the hardest muon for the signal (all BPs)

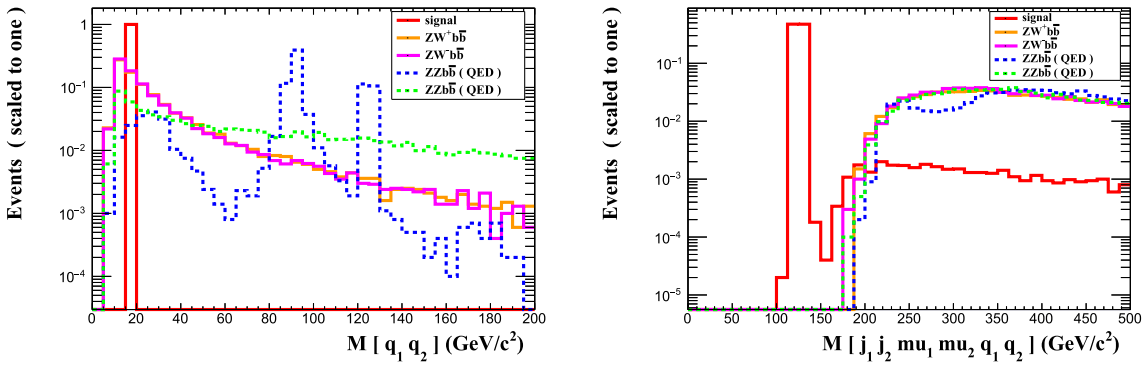

Fig. 8 The invariant mass of the $b\bar{b}$ (left) and $\mu^+\mu^-\ jj\ b\bar{b}$ (right) system for the signal (BP1) and the irreducible backgrounds ($ZZb\bar{b}$, $ZWb\bar{b}$) at parton level

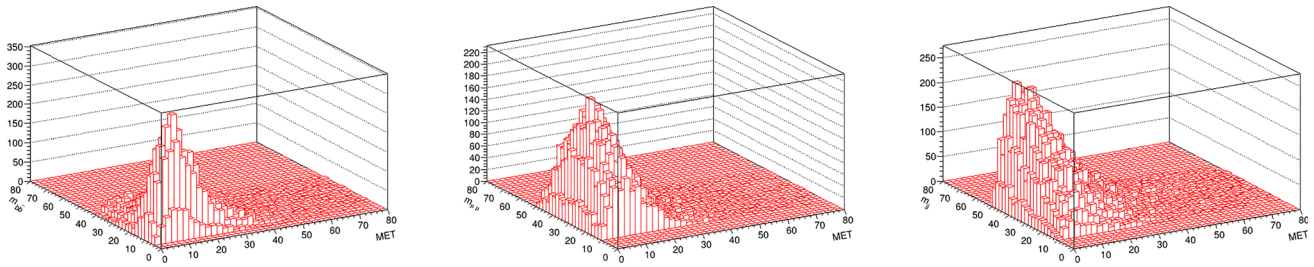

Fig. 9 Correlation between $\not{E}_T$ and $m_{b\bar{b}}$ (left panel), $m_{\mu\mu}$ (middle panel) and m_{jj} (right panel) for signal (BP3), at detector level

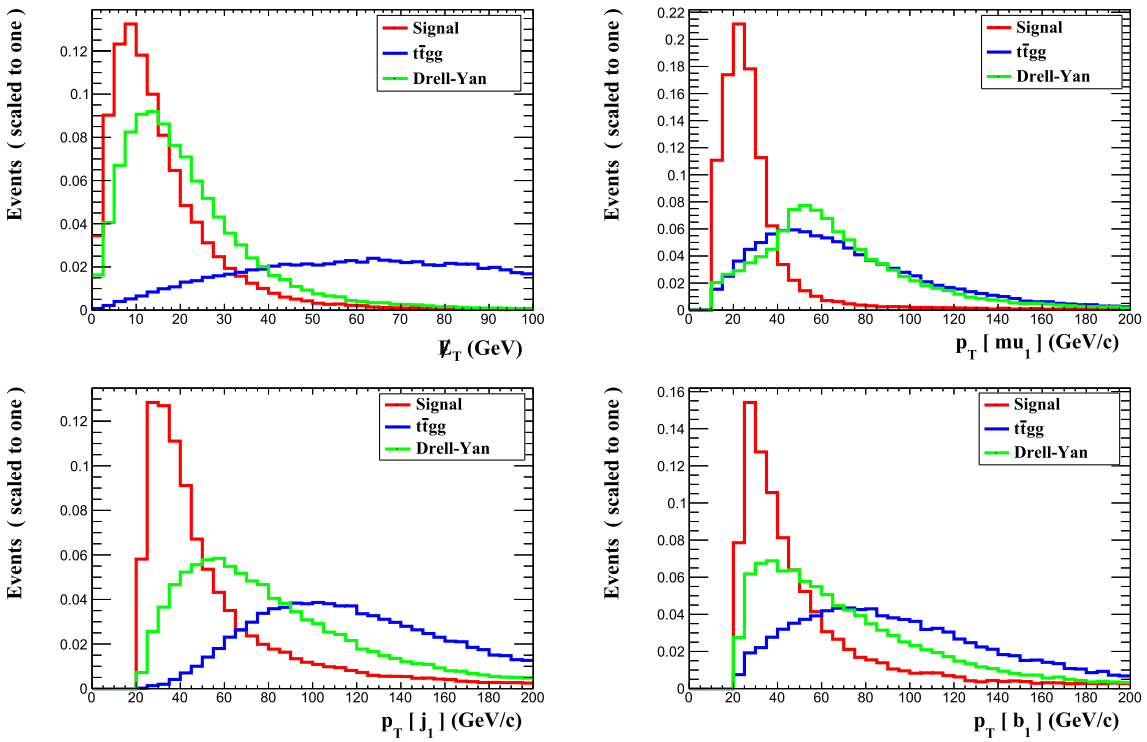

Fig. 10 The $\not{E}_T$ and highest p_T distributions for muons, b- and light-jets (clockwise) for signal (BP3) and background processes, $ggt\bar{t}$ (blue) and DY+jets (green), at detector level

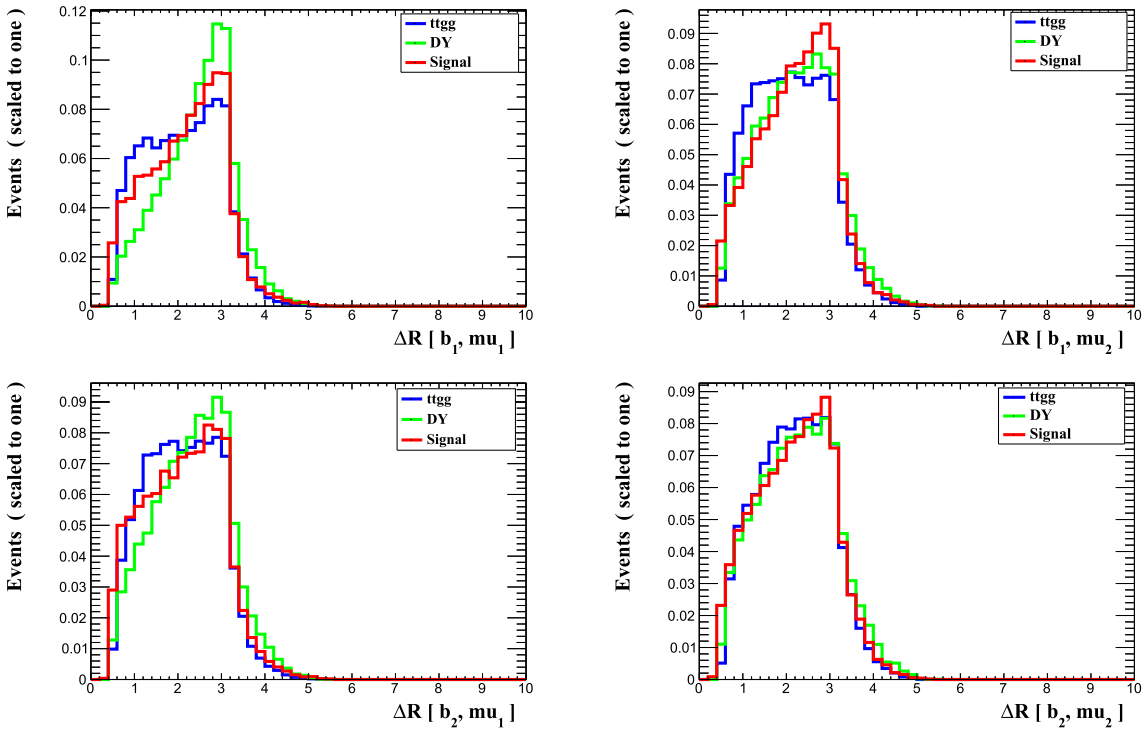

Fig. 11 ΔR distributions between the two (p_T ordered) b-jets and muons, from hardest to softest (clockwise) for signal (red) (BP3) and background processes, $ggt\bar{t}$ (blue) and DY+jets (green), at detector level

The $\not{E}_{\rm T}$ distribution from simulated samples of background events is mainly from di-leptonic decay of $ggt\bar{t}$, i.e., with $t\bar{t} \to W^+bW^-\bar{b} \to (\mu^+\nu_\mu b)(\mu^-\bar{\nu}_\mu\bar{b})$ whereas the $\not{E}_{\rm T}$ in both signal and DY+jets events is due to the semi-leptonic b-meson decays (alongside detector effects). Furthermore, Fig. 11 illustrates the different angular separations between b-quarks and muons for signal and dominant backgrounds, where one can read that background arsing from top pair production has only a minimal component with muons coming from semi-leptonic b-meson decays (as intimated).

To enhance the signals and suppress the backgrounds arising from $ggt\bar{t}$ and DY+jets, we have adopted several kinematic cuts, which choice is based on comparing different distributions of the signal and background processes at the detector level. Specifically, this has been done through 2D distributions correlating the missing transverse momentum to a series of kinematic variables pertaining to some of the visible objects in the final state as illustrated in Figs. 12 and 13 for signal and background processes mentioned above. One can read that the signal and backgrounds distributions are anti-correlated. In fact, forcing the missing transverse energy to be below 30 GeV will strongly favour the signal over the backgrounds, specifically, $ggt\bar{t}$.[11] Additionally, selecting events with $p_T^j < 75$ GeV and $p_T^\mu < 40$ GeV would enhance the signal significance and suppress both background processes. Through similar reasoning, we require the invariant mass of the system to satisfy $m_H < 180$ GeV. We show in Table 5 the event rates of the backgrounds after applying the cutflow discussed above. Notably, DY+jets events are significantly reduced after considering a final state with exactly 2 b-jets, 2 light jets and 2 muons, while adhering to the invariant masses requirements.[12] Both backgrounds processes are completely removed after applying the kinematic cuts and restricting the invariant mass of the system to be below 180 GeV to further differentiate the signal from the remaining background processes.

We have then computed the significance (for $\sqrt{s} = 13$ TeV and $\mathcal{L} = 300$ fb^{-1}), defined as $\Sigma = \frac{S}{\sqrt{B+S}} = \sqrt{S}$,[13] where $S(B)$ is the signal(background) yield after the discussed cutflow, for not only our three initial BPs (whose Σ rates are 3.05, 3.18 and 3.42 for BP1, BP2 and BP3, respectively), but also those appearing in Table 6. We have done so in order to be able to map the 2HDM Type-I parameter space in detail, so as to acquire a sense of the true portion of it that can be tested by forthcoming experiments. Note that

[11] Only 10% of $t\bar{t}gg$ events have survived after applying the missing transverse energy cut, as indicated in Table 5.

[12] $b\bar{b}$ originate from a light Higgs (h) decay with $m_h < 40$ GeV. We therefore set a cut on the invariant mass of $b\bar{b}$ to capture the light Higgs of the signal as illustrated in the right panel of Fig. 9, and to suppress the backgrounds.

[13] The major background processes, $t\bar{t}gg$ and DY+jets, are suppressed once the kinematic cuts are implemented.

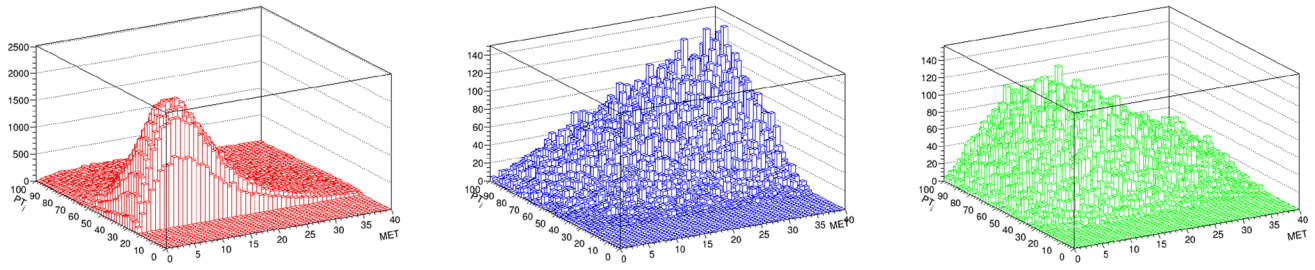

Fig. 12 Correlation between p_T^j and $\not{E}_{\rm T}$ for signal (BP3) (red), $ggt\bar{t}$ (blue) and DY+jets (green) at detector level

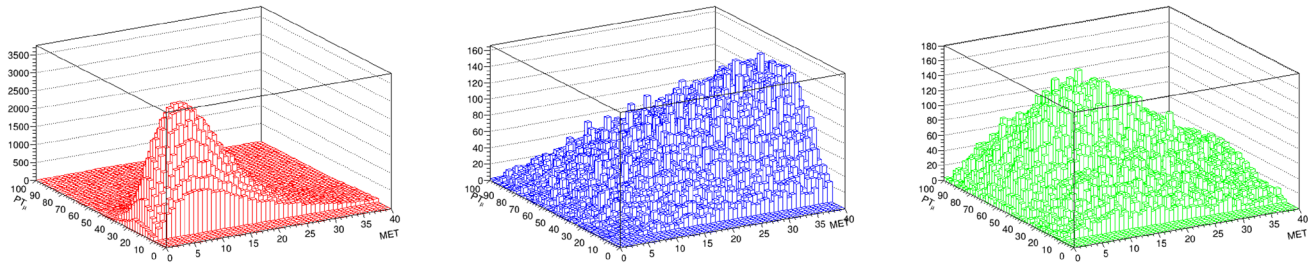

Fig. 13 Correlation between p_T^μ and $\not{E}_{\rm T}$ for signal (BP3) (red colour), $ggt\bar{t}$ (blue colour) and DY+jets (green colour) at detector level

Table 5 Event rates of the two dominant background processes, $ggt\bar{t}$ and DY+jets, with $\sqrt{s} = 13$ TeV and $\mathcal{L} = 300$ fb^{-1} after applying the cutflow

Cutflow	DY+jets	$t\bar{t}gg$
Number of events $(\mathcal{L}, \sigma)$	960,000.000	534,000.000
$\not{E}_{\rm T} < 30.0$ GeV	743,769.811	56,336.998
$\mu^\pm\mu^\mp$, $m_{\mu\mu} \in [10,\ 50]$ GeV	46022.406	5521.560
2 light jets, $m_{jj} \in [10,\ 50]$ GeV	5952.001	1655.400
2 b-jets, $m_{b\bar{b}} \in [5,\ 40]$ GeV	19.200	21.360
$p_T^j < 70$ GeV	19.200	21.360
$p_T^\mu < 50$ GeV	19.200	0.00

we have kept the same cutflow already illustrated for all such new BPs too. Also, it is at this stage that we take into account the aforementioned QCD K-factor for the signal. Many of the latter can have a significance larger than 3 and up to nearly 4, for Run 3 energy and luminosity. To observe their distribution over the (m_h, m_a) plane, we have finally produced Fig. 14, indeed, assuming $\sqrt{s} = 13$ TeV and $\mathcal{L} = 300$ fb^{-1}, where both significance (Σ) and efficiency (ϵ) are mapped. Hence, at Run 3, we can conclude that a substantial portion of the 2HDM Type-I parameter space can offer some evidence of the signal we have pursued. Furthermore, we notice that a larger efficiency can be obtained for small m_a: this is because the loss of efficiency with b-tagging is over-compensated by a simultaneous higher efficiency for both j- and μ-tagging. Needless to say, at the HL-LHC, where $\mathcal{L} = 3000$ fb^{-1}, most of the sampled parameter space of the 2HDM Type-I would be discoverable.

5 Conclusions

In this paper, we have shown the outcome of performing some recasting over the parameter space of the 2HDM Type I, wherein the heaviest CP-even Higgs state H is identified with the discovered SM-like one, $H_{\rm SM}$, while h and a are lighter. After considering the available experimental data from searches for exotic Higgs decay into two light (pseudo)scalars, we have found that the corresponding parameter space for which there is sensitivity via $H_{\rm SM} \to hh(aa) \to \tau^+\tau^- b\bar{b}$ at Run 2 is already excluded by existing constraints from BSM Higgs searches. Furthermore, we have shown that there are regions of the 2HDM Type-I parameter space compliant with theoretical and experimental constraints yielding substantial BR$(H^\pm \to W^\pm a)$ and BR$(H \to Z^*Z^*h)$. The large size of the former has been exploited in other literature. Here, concerning the lat-

Table 6 Extended list of BPs used in the MC simulation for the 2HDM Type-I parameter scan, highlighting the h and a masses as well as the signal LO cross section and event rate after the full cutflow, together with its significance Σ and efficiency ϵ. Recall that NNLO QCD K-factor has been used for Higgs production. Here, $\sqrt{s} = 13$ TeV and $\mathcal{L} = 300$ fb^{-1}

BP	m_h (GeV)	m_a (GeV)	σ (pb)	No. of events	Significance Σ	Efficiency ϵ
BP4	11.85	72.75	4.82×10^{-4}	12.94	3.59	0.033
BP5	17.15	76.24	2.54×10^{-4}	6.9695	2.63	0.035
BP6	24.55	78.85	1.39×10^{-4}	3.5894	1.89	0.032
BP7	15.98	82.43	1.705×10^{-4}	4.8392	2.19	0.036
BP8	34.15	84.26	4.48×10^{-5}	1.22	1.10	0.034
BP9	20.69	79.30	2.30×10^{-4}	7.2086	2.68	0.039
BP10	16.73	71.67	3.31×10^{-4}	8.7579	2.95	0.033
BP11	16.78	69.25	3.247×10^{-4}	8.8105	2.96	0.034
BP12	21.82	85.56	1.42×10^{-4}	3.66	1.91	0.032
BP13	22.78	77.17	1.629×10^{-4}	5.34	2.31	0.041
BP14	17.09	78.40	2.038×10^{-4}	5.81	2.41	0.037
BP15	19.10	72.89	2.401×10^{-4}	6.94	2.63	0.043
BP16	15.87	75.024	2.192×10^{-4}	4.19	2.04	0.025
BP17	15.67	78.38	2.426×10^{-4}	4.32	2.07	0.023
BP18	19.76	83.14	1.662×10^{-4}	3.22	1.79	0.025
BP19	20.24	76.76	1.873×10^{-4}	4.76	2.18	0.032
BP20	28.15	77.04	9.39×10^{-5}	2.37	1.53	0.032
BP21	27.085	79.40	8.134×10^{-5}	1.67	1.29	0.027
BP22	11.83	74.06	4.577×10^{-4}	13.34	3.65	0.036
BP23	12.285	76.51	3.377×10^{-4}	10.30	3.20	0.035
BP24	13.09	75.47	3.538×10^{-4}	10.01	3.16	0.035
BP25	14.15	74.35	3.458×10^{-4}	9.24	3.03	0.034
BP26	11.96	78.57	3.557×10^{-4}	9.33	3.04	0.033
BP27	12.60	77.17	3.311×10^{-4}	9.92	3.14	0.038
BP28	14.30	76.77	2.423×10^{-4}	6.46	2.54	0.034
BP29	14.16	78.86	2.572×10^{-4}	5.75	2.39	0.036
BP30	16.15	81.22	1.843×10^{-4}	5.11	2.26	0.028
BP31	12.85	83.93	2.308×10^{-4}	5.13	2.26	0.028
BP32	11.63	88.72	1.325×10^{-4}	2.57	1.60	0.025
BP33	19.86	88.73	8.03×10^{-5}	1.67	1.29	0.027
BP34	22.71	74.16	1.093×10^{-4}	3.28	1.81	0.039

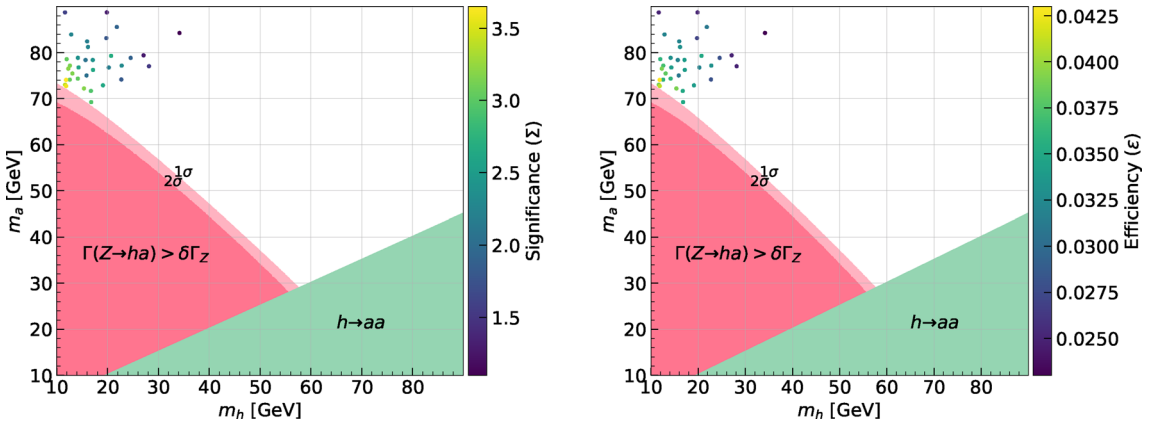

Fig. 14 Significance (left) and efficiency (right) of each BP produced in our analysis over the (m_h, m_a) projection of the 2HDM Type-I parameter space, after the full cutflow described in the text

ter, we have made the case for looking at the process $pp \to H_{\rm SM} \to Z^*A \to Z^*Z^*h$ via $ZZ \to \mu^+\mu^- jj$ and $h \to b\bar{b}$ decays, specifically, in the region with large m_a and small m_h. After performing a full MC analysis down to detector level, we have proven that the overwhelming backgrounds arising from both top-quark pair production in association with 2 ISR jets and DY+jets can be suppressed after applying efficient kinematics cuts, leading to a large significance of this hitherto unexplored light Higgs signature already at Run 3 of the LHC, where evidence of it can be seen, further affording one with clear discovery potential at the HL-LHC.

Acknowledgements The work of SM is supported in part through the NExT Institute and the STFC Consolidated Grant No. ST/L000296/1. SS is fully supported through the NExT Institute. SS acknowledges the use of the IRIDIS High Performance Computing Facility, and associated support services at the University of Southampton, in the completion of this work.

Data availability statement This manuscript has no associated data or the data will not be deposited. [Authors' comment: This is a theoretical study that has no associated data.]

Code availability My manuscript has no associated code/software. [Authors' comment: This is a theoretical study that has no associated code/software.]

Funded by SCOAP[3].

References

1. ATLAS, CMS collaboration, Measurements of the Higgs boson production and decay rates and constraints on its couplings from a combined ATLAS and CMS analysis of the LHC pp collision data at $\sqrt{s} = 7$ and 8 TeV. JHEP**08**, 045 (2016). https://doi.org/10.1007/JHEP08(2016)045. arXiv:1606.02266
2. shape ATLAS collaboration, A detailed map of Higgs boson interactions by the ATLAS experiment ten years after the discovery. Nat. Ser. **607**, 52 (2022). https://doi.org/10.1038/s41586-022-04893-w. arXiv:2207.00092
3. shape CMS collaboration, A portrait of the Higgs boson by the CMS experiment ten years after the discovery. Nat. Ser. **607**, 60 (2022). https://doi.org/10.1038/s41586-022-04892-x. arXiv:2207.00043
4. CMS, ATLAS collaboration, Evidence for the Higgs boson decay to a Z boson and a photon at the LHC. arXiv:2309.03501
5. CMS collaboration, A search for decays of the Higgs boson to invisible particles in events with a top-antitop quark pair or a vector boson in proton-proton collisions at $\sqrt{s}$ = 13 TeV. arXiv:2303.01214
6. shape ATLAS collaboration, Combination of searches for invisible decays of the Higgs boson using 139 fb^{-1} of proton-proton collision data at $\sqrt{s} = 13$ TeV collected with the ATLAS experiment. Phys. Lett. B Ser. **842**, 137963 (2023). https://doi.org/10.1016/j.physletb.2023.137963. arXiv:2301.10731
7. shape CMS collaboration, Search for invisible decays of a Higgs boson produced through vector boson fusion in proton-proton collisions at $\sqrt{s} = 13$ TeV. Phys. Lett. B Ser. **793**, 520 (2019). https://doi.org/10.1016/j.physletb.2019.04.025. arXiv:1809.05937
8. shape ATLAS collaboration, Search for invisible Higgs-boson decays in events with vector-boson fusion signatures using 139 fb^{-1} of proton-proton data recorded by the ATLAS experiment. JHEP series **08**, 104 (2022). https://doi.org/10.1007/JHEP08(2022)104. arXiv:2202.07953
9. T.D. Lee, A Theory of Spontaneous T Violation. Phys. Rev. D Ser. **8**, 1226 (1973). https://doi.org/10.1103/PhysRevD.8.1226
10. J.F. Gunion, H.E. Haber, G.L. Kane, S. Dawson, *The Higgs Hunter's Guide*, vol. 80 (2000)
11. J.F. Gunion, H.E. Haber, G.L. Kane, S. Dawson, *Errata for the Higgs hunter's guide*. arXiv:hep-ph/9302272
12. M. Aoki, S. Kanemura, K. Tsumura, K. Yagyu, Models of Yukawa interaction in the two Higgs doublet model, and their collider phenomenology. Phys. Rev. D Ser. **80**, 015017 (2009). https://doi.org/10.1103/PhysRevD.80.015017. arXiv:0902.4665
13. G.C. Branco, P.M. Ferreira, L. Lavoura, M.N. Rebelo, M. Sher, J.P. Silva, Theory and phenomenology of two-Higgs-doublet models. Phys. Rept. Ser. **516**, 1 (2012). https://doi.org/10.1016/j.physrep.2012.02.002. arXiv:1106.0034
14. C.-Y. Chen, M. Freid, M. Sher, Next-to-minimal two Higgs doublet model. Phys. Rev. D Ser. **89**, 075009 (2014). https://doi.org/10.1103/PhysRevD.89.075009. arXiv:1312.3949
15. M. Muhlleitner, M.O.P. Sampaio, R. Santos, J. Wittbrodt, The N2HDM under theoretical and experimental scrutiny. JHEP Ser. **03**, 094 (2017). https://doi.org/10.1007/JHEP03(2017)094. arXiv:1612.01309
16. I. Engeln, M. Mühlleitner, J. Wittbrodt, N2HDECAY: Higgs boson decays in the different phases of the N2HDM. Comput. Phys. Commun. series **234**, 256 (2019). https://doi.org/10.1016/j.cpc.2018.07.020. arXiv:1805.00966
17. A. Arhrib, R. Benbrik, M. El Kacimi, L. Rahili, S. Semlali, Extended Higgs sector of 2HDM with real singlet facing LHC data. Eur. Phys. J. C Ser. **80**, 13 (2020). https://doi.org/10.1140/epjc/s10052-019-7472-2. arXiv:1811.12431
18. R. Barbieri, S. Ferrara, C.A. Savoy, Gauge Models with Spontaneously Broken Local Supersymmetry. Phys. Lett. B Ser. **119**, 343 (1982). https://doi.org/10.1016/0370-2693(82)90685-2
19. J.R. Ellis, J.F. Gunion, H.E. Haber, L. Roszkowski, F. Zwirner, Higgs Bosons in a Nonminimal Supersymmetric Model. Phys. Rev. D Ser. **39**, 844 (1989). https://doi.org/10.1103/PhysRevD.39.844
20. U. Ellwanger, M. Rausch de Traubenberg, C.A. Savoy, Particle spectrum in supersymmetric models with a gauge singlet. Phys. Lett. B Ser. **315**, 331 (1993). https://doi.org/10.1016/0370-2693(93)91621-S. arXiv:hep-ph/9307322
21. T. Elliott, S.F. King, P.L. White, Unification constraints in the next-to-minimal supersymmetric standard model. Phys. Lett. B Ser. **351**, 213 (1995). https://doi.org/10.1016/0370-2693(95)00381-T. arXiv:hep-ph/9406303
22. M. Maniatis, The next-to-minimal supersymmetric extension of the standard model reviewed. Int. J. Mod. Phys. A Ser. **25**, 3505 (2010). https://doi.org/10.1142/S0217751X10049827. arXiv:0906.0777
23. U. Ellwanger, C. Hugonie, A.M. Teixeira, The Next-to-Minimal Supersymmetric Standard Model. Phys. Rept. Ser. **496**, 1 (2010). https://doi.org/10.1016/j.physrep.2010.07.001. arXiv:0910.1785

24. S. Moretti, S. Khalil, *Supersymmetry Beyond Minimality: From Theory to Experiment*, CRC Press (2019)
25. S.L. Glashow, S. Weinberg, Natural conservation laws for neutral currents. Phys. Rev. D Ser. **15**, 1958 (1977). https://doi.org/10.1103/PhysRevD.15.1958
26. E.A. Paschos, Diagonal neutral currents. Phys. Rev. D Ser. **15**, 1966 (1977). https://doi.org/10.1103/PhysRevD.15.1966
27. M. Misiak, A. Rehman, M. Steinhauser, Towards $\overline{B} \to X_s\gamma$ at the NNLO in QCD without interpolation in m_c. JHEP Ser. **06**, 175 (2020). https://doi.org/10.1007/JHEP06(2020)175. arXiv:2002.01548
28. S. Kanemura, T. Kubota, E. Takasugi, Lee-Quigg-Thacker bounds for Higgs boson masses in a two doublet model. Phys. Lett. B Ser. **313**, 155 (1993). https://doi.org/10.1016/0370-2693(93)91205-2. arXiv:hep-ph/9303263
29. A.G. Akeroyd, A. Arhrib, E.-M. Naimi, Note on tree level unitarity in the general two Higgs doublet model. Phys. Lett. B Ser. **490**, 119 (2000). https://doi.org/10.1016/S0370-2693(00)00962-X. arXiv:hep-ph/0006035
30. A. Arhrib, *Unitarity constraints on scalar parameters of the standard and two Higgs doublets model*, in *Workshop on Noncommutative Geometry, Superstrings and Particle Physics*, 12 (2000). arXiv:hep-ph/0012353
31. A.W. El Kaffas, W. Khater, O.M. Ogreid, P. Osland, Consistency of the two Higgs doublet model and CP violation in top production at the LHC. Nucl. Phys. B Ser. **775**, 45 (2007). https://doi.org/10.1016/j.nuclphysb.2007.03.041. arXiv:hep-ph/0605142
32. D. Eriksson, J. Rathsman, O. Stal, 2HDMC: Two-Higgs-Doublet Model Calculator Physics and Manual. Comput. Phys. Commun. Ser. **181**, 189 (2010). https://doi.org/10.1016/j.cpc.2009.09.011. arXiv:0902.0851
33. M.E. Peskin, T. Takeuchi, A New constraint on a strongly interacting Higgs sector. Phys. Rev. Lett. Ser. **65**, 964 (1990). https://doi.org/10.1103/PhysRevLett.65.964
34. M.E. Peskin, T. Takeuchi, Estimation of oblique electroweak corrections. Phys. Rev. D Ser. **46**, 381 (1992). https://doi.org/10.1103/PhysRevD.46.381
35. Particle Data Group collaboration, *Rev. Part. Phys. PTEP***2022**, 083C01 (2022). https://doi.org/10.1093/ptep/ptac097
36. ALEPH, DELPHI, L3, OPAL, SLD, LEP Electroweak Working Group, SLD Electroweak Group, SLD Heavy Flavour Group collaboration, Precision electroweak measurements on the Z resonance. Phys. Rept. **427**, 257 (2006). https://doi.org/10.1016/j.physrep.2005.12.006. arXiv:hep-ex/0509008
37. P. Janot, S. Jadach, Improved Bhabha cross section at LEP and the number of light neutrino species. Phys. Lett. B Ser. **803**, 135319 (2020). https://doi.org/10.1016/j.physletb.2020.135319. arXiv:1912.02067
38. P. Bechtle, D. Dercks, S. Heinemeyer, T. Klingl, T. Stefaniak, G. Weiglein et al., HiggsBounds-5: Testing Higgs Sectors in the LHC 13 TeV Era. Eur. Phys. J. C Ser. **80**, 1211 (2020). https://doi.org/10.1140/epjc/s10052-020-08557-9. arXiv:2006.06007
39. P. Bechtle, S. Heinemeyer, T. Klingl, T. Stefaniak, G. Weiglein, J. Wittbrodt, HiggsSignals-2: Probing new physics with precision Higgs measurements in the LHC 13 TeV era. Eur. Phys. J. C Ser. **81**, 145 (2021). https://doi.org/10.1140/epjc/s10052-021-08942-y. arXiv:2012.09197
40. F. Mahmoudi, SuperIso v2.3: A program for calculating flavor physics observables in supersymmetry. Comput. Phys. Commun. **180**, 1579 (2009). https://doi.org/10.1016/j.cpc.2009.02.017. arXiv:0808.3144
41. shape HFLAV collaboration, Averages of b-hadron, c-hadron, and τ-lepton properties as of summer 2016. Eur. Phys. J. C Ser. **77**, 895 (2017). https://doi.org/10.1140/epjc/s10052-017-5058-4. arXiv:1612.07233
42. shape LHCb collaboration, Measurement of the $B_s^0 \to \mu^+\mu^-$ decay properties and search for the $B^0 \to \mu^+\mu^-$ and $B_s^0 \to \mu^+\mu^-\gamma$ decays. Phys. Rev. D Ser. **105**, 012010 (2022). https://doi.org/10.1103/PhysRevD.105.012010. arXiv:2108.09283
43. shape LHCb collaboration, Analysis of Neutral B-Meson Decays into Two Muons. Phys. Rev. Lett. Ser. **128**, 041801 (2022). https://doi.org/10.1103/PhysRevLett.128.041801. arXiv:2108.09284
44. shape CMS collaboration, Measurement of the $B_S^0 \to \mu^+\mu^-$ decay properties and search for the $B^0 \to \mu^+\mu^-$ decay in proton-proton collisions at $\sqrt{s}$ = 13 TeV. Phys. Lett. B Ser. **842**, 137955 (2023). https://doi.org/10.1016/j.physletb.2023.137955. arXiv:2212.10311
45. shape CMS collaboration, Search for an exotic decay of the Higgs boson to a pair of light pseudoscalars in the final state with two muons and two b quarks in pp collisions at 13 TeV. Phys. Lett. B Ser. **795**, 398 (2019). https://doi.org/10.1016/j.physletb.2019.06.021. arXiv:1812.06359
46. shape ATLAS collaboration, Search for Higgs boson decays into a pair of light bosons in the $bb\mu\mu$ final state in pp collision at $\sqrt{s} = 13$ TeV with the ATLAS detector. Phys. Lett. B Ser. **790**, 1 (2019). https://doi.org/10.1016/j.physletb.2018.10.073. arXiv:1807.00539
47. shape CMS collaboration, Search for an exotic decay of the Higgs boson to a pair of light pseudoscalars in the final state of two muons and two τ leptons in proton-proton collisions at $\sqrt{s} = 13$ TeV. JHEP Ser. **11**, 018 (2018). https://doi.org/10.1007/JHEP11(2018)018. arXiv:1805.04865
48. shape CMS collaboration, Search for an exotic decay of the Higgs boson to a pair of light pseudoscalars in the final state with two b quarks and two τ leptons in proton-proton collisions at $\sqrt{s} = 13$ TeV. Phys. Lett. B Ser. **785**, 462 (2018). https://doi.org/10.1016/j.physletb.2018.08.057. arXiv:1805.10191
49. CMS collaboration, *Search for exotic decay of the Higgs boson into two light pseudoscalars with four photons in the final state at* $\sqrt{s}$ *= 13 TeV*, *CMS-PAS-HIG-21-003* (2021)
50. P. Uwer, *EasyNData: A Simple tool to extract numerical values from published plots*. arXiv:0710.2896
51. CMS collaboration, Search for exotic Higgs boson decays to a pair of pseudoscalars in the $\mu\mu$bb and $\tau\tau$bb final states in proton-proton collisions with the CMS experiment. CMS-PAS-HIG-22-007 (2023)
52. shape CMS collaboration, Search for a light pseudoscalar Higgs boson in the boosted $\mu\mu\tau\tau$ final state in proton-proton collisions at $\sqrt{s} = 13$ TeV. JHEP Ser. **08**, 139 (2020). https://doi.org/10.1007/JHEP08(2020)139. arXiv:2005.08694
53. shape ATLAS collaboration, Search for Higgs boson decays into a pair of pseudoscalar particles in the $bb\mu\mu$ final state with the ATLAS detector in pp collisions at $\sqrt{s}$=13 TeV. Phys. Rev. D Ser. **105**, 012006 (2022). https://doi.org/10.1103/PhysRevD.105.012006. arXiv:2110.00313
54. ALEPH, DELPHI, L3, OPAL, LEP Working Group for Higgs Boson Searches collaboration, *Search for neutral MSSM Higgs bosons at LEP*. Eur. Phys. J. C **47**, 547 (2006). https://doi.org/10.1140/epjc/s2006-02569-7. arXiv:hep-ex/0602042
55. shape ATLAS collaboration, Search for new phenomena in events with at least three photons collected in pp collisions at $\sqrt{s}$ = 8 TeV with the ATLAS detector. Eur. Phys. J. C Ser. **76**, 210 (2016). https://doi.org/10.1140/epjc/s10052-016-4034-8. arXiv:1509.05051
56. S. Semlali, H. Day-Hall, S. Moretti, R. Benbrik, Mapping $pp \to A \to ZH \to l^+l^-b\bar{b}$ and $pp \to H \to ZA \to l^+l^-b\bar{b}$ current and future searches onto 2HDM parameter spaces. Phys. Lett. B Ser. **810**, 135819 (2020). https://doi.org/10.1016/j.physletb.2020.135819. arXiv:2006.05177

57. A.G. Akeroyd, Three body decays of Higgs bosons at LEP-2 and application to a hidden fermiophobic Higgs. Nucl. Phys. B Ser. **544**, 557 (1999). https://doi.org/10.1016/S0550-3213(98)00845-1. arXiv:hep-ph/9806337
58. A. Arhrib, R. Benbrik, S. Moretti, Bosonic Decays of Charged Higgs Bosons in a 2HDM Type-I. Eur. Phys. J. C Ser. **77**, 621 (2017). https://doi.org/10.1140/epjc/s10052-017-5197-7. arXiv:1607.02402
59. A. Arhrib, R. Benbrik, M. Krab, B. Manaut, S. Moretti, Y. Wang et al., New discovery modes for a light charged Higgs boson at the LHC. JHEP Ser. **10**, 073 (2021). https://doi.org/10.1007/JHEP10(2021)073. arXiv:2106.13656
60. Y. Wang, A. Arhrib, R. Benbrik, M. Krab, B. Manaut, S. Moretti et al., Analysis of $W^{\pm}+4\gamma$ in the 2HDM Type-I at the LHC. JHEP Ser. **12**, 021 (2021). https://doi.org/10.1007/JHEP12(2021)021. arXiv:2107.01451
61. ATLAS collaboration, Search for $H^{\pm} \to W^{\pm}A \to W^{\pm}\mu\mu$ in $pp \to t\bar{t}$ events using an $e\mu\mu$ signature with the ATLAS detector at $\sqrt{s} = 13$ TeV, *ATLAS-CONF-2021-047* (2021)
62. shape CMS collaboration, Search for a light charged Higgs boson decaying to a W boson and a CP-odd Higgs boson in final states with $e\mu\mu$ or $\mu\mu\mu$ in proton-proton collisions at $\sqrt{s} = 13$ TeV. Phys. Rev. Lett. Ser. **123**, 131802 (2019). https://doi.org/10.1103/PhysRevLett.123.131802. arXiv:1905.07453
63. CDF collaboration, Search for charged Higgs bosons from top quark decays in $p\bar{p}$ collisions at $\sqrt{s} = 1.96$-TeV. Phys. Rev. Lett. **96**, 042003 (2006). https://doi.org/10.1103/PhysRevLett.96.042003. arXiv:hep-ex/0510065
64. CDF collaboration, Search for a Very Light CP-Odd Higgs Boson in Top Quark Decays from $p^{-}p$Collisions at 1.96 TeV. Phys. Rev. Lett. **107**, 031801 (2011). https://doi.org/10.1103/PhysRevLett.107.031801. arXiv:1104.5701
65. shape OPAL collaboration, Search for Charged Higgs Bosons in $e^{+}e^{-}$ Collisions at $\sqrt{s} = 189--209$ GeV. Eur. Phys. J. C Ser. **72**, 2076 (2012). https://doi.org/10.1140/epjc/s10052-012-2076-0. arXiv:0812.0267
66. ALEPH, DELPHI, L3, OPAL, LEP collaboration, Search for Charged Higgs bosons: Combined Results Using LEP Data. Eur. Phys. J. C **73**, 2463 (2013). https://doi.org/10.1140/epjc/s10052-013-2463-1. arXiv:1301.6065
67. R.V. Harlander, S. Liebler, H. Mantler, SusHi: A program for the calculation of Higgs production in gluon fusion and bottom-quark annihilation in the Standard Model and the MSSM. Comput. Phys. Commun. Ser. **184**, 1605 (2013). https://doi.org/10.1016/j.cpc.2013.02.006. arXiv:1212.3249
68. R.V. Harlander, S. Liebler, H. Mantler, SusHi Bento: Beyond NNLO and the heavy-top limit. Comput. Phys. Commun. Ser. **212**, 239 (2017). https://doi.org/10.1016/j.cpc.2016.10.015. arXiv:1605.03190
69. R.V. Harlander, W.B. Kilgore, Next-to-next-to-leading order Higgs production at hadron colliders. Phys. Rev. Lett. Ser. **88**, 201801 (2002). https://doi.org/10.1103/PhysRevLett.88.201801. arXiv:hep-ph/0201206
70. J. Alwall, R. Frederix, S. Frixione, V. Hirschi, F. Maltoni, O. Mattelaer et al., The automated computation of tree-level and next-to-leading order differential cross sections, and their matching to parton shower simulations. JHEP Ser. **07**, 079 (2014). https://doi.org/10.1007/JHEP07(2014)079. arXiv:1405.0301
71. G. Bevilacqua, M. Czakon, C.G. Papadopoulos, M. Worek, Hadronic top-quark pair production in association with two jets at Next-to-Leading Order QCD. Phys. Rev. D Ser. **84**, 114017 (2011). https://doi.org/10.1103/PhysRevD.84.114017. arXiv:1108.2851
72. T. Sjostrand, S. Mrenna, P.Z. Skands, PYTHIA 6.4 Physics and Manual. JHEP**05**, 026 (2006). https://doi.org/10.1088/1126-6708/2006/05/026. arXiv:hep-ph/0603175
73. DELPHES 3 collaboration, DELPHES 3, A modular framework for fast simulation of a generic collider experiment. JHEP **02**, 057 (2014). https://doi.org/10.1007/JHEP02(2014)057. arXiv:1307.6346
74. E. Conte, B. Fuks, G. Serret, MadAnalysis 5, A user-friendly framework for collider phenomenology. Comput. Phys. Commun. Ser. **184**, 222 (2013). https://doi.org/10.1016/j.cpc.2012.09.009. arXiv:1206.1599
75. E. Accomando, L. Delle Rose, S. Moretti, E. Olaiya, C.H. Shepherd-Themistocleous, Novel SM-like Higgs decay into displaced heavy neutrino pairs in U(1)' models. JHEP **04**, 081 (2017). https://doi.org/10.1007/JHEP04(2017)081. arXiv:1612.05977
76. shape CMS collaboration, Performance of the CMS muon trigger system in proton-proton collisions at $\sqrt{s} = 13$ TeV. JINST Ser. **16**, P07001 (2021). https://doi.org/10.1088/1748-0221/16/07/P07001. arXiv:2102.04790
77. shape CMS collaboration, Search for a Narrow Resonance Lighter than 200 GeV Decaying to a Pair of Muons in Proton-Proton Collisions at $\sqrt{s} = 13$ TeV. Phys. Rev. Lett. Ser. **124**, 131802 (2020). https://doi.org/10.1103/PhysRevLett.124.131802. arXiv:1912.04776
78. CMS collaboration, Search for prompt production of a GeV scale resonance decaying to a pair of muons in proton-proton collisions at $\sqrt{s} = 13$TeV. *CMS-PAS-EXO-21-005* (2023)
79. CMS collaboration, *Dimuon scouting at CMS. CMS-DP-2023-070* (2023)